Copyright 2019 Society of Photo-Optical Instrumentation Engineers. One print or electronic copy may be made for personal use only. Systematic reproduction and distribution, duplication of any material in this paper for a fee or for commercial purposes, or modification of the content of the paper are prohibited. https://doi.org/10.1117/12.2525584

Imaging detection and classification of particulate contamination on structured surfaces

Jan Schütz*, Alexander Blättermann, Peter Kozlowski, Albrecht Brandenburg
Fraunhofer-Institute for Physical Measurement Techniques IPM, Heidenhofstrasse 8, 79110 Freiburg, Germany

ABSTRACT

We present new imaging techniques for the detection and classification of particulate contamination on structured surfaces. This allows for cleanliness inspection directly on the sample.

Classical imaging techniques for particle detection, such as dark-field imaging, are typically limited to flat surfaces because structures, scratches, or rough surfaces will give similar signals as particles. This problem is overcome using stimulated differential imaging. Stimulation of the sample, e.g. by air blasts, results in displacement of only the particles while sample structures remain in place. Thus, the difference of images before and after stimulation reveals the particles with high contrast.

Cleanliness inspection systems also need to distinguish (often harmful) metallic particles from (often harmless) non-metallic particles. A recognized classification method is measuring gloss. When illuminated with directed light, the glossy surface of metallic particles directly reflects most parts of the light. Non-metallic particles, in contrast, typically scatter most of the light uniformly. Here, we demonstrate a new imaging technique to measure gloss. For this purpose, several images of the sample with different angles of illumination are taken and analyzed for similarity.

Keywords: cleanliness inspection, particle detection, inline measurement technique, production control

INTRODUCTION

Technical cleanliness is a decisive criterion for the service life of highly stressed components. In the production process, it is typically distinguished between filmic and particulate contaminations. Liquid impurities, such as residues of lubricants, detergents, corrosion inhibitor, and further process additives, are classified as filmic contaminants. They are especially harmful when further process steps include gluing or painting. Solid impurities, in contrast, are classified as particulate contaminants. They originate typically from machining, assembly, handling, textile fibers, or dust. Different methods have been established for cleanliness inspection of filmic and particulate contaminations [1,2]. In the following, we will focus on particulate contaminations.

Depending on the type of product, different sizes of particulate contaminations are critical. In the automotive industry, for example, particles with size 50 µm to 2 mm are typically considered. In the pharmaceutical and semiconductor industries, significantly smaller particles are relevant.

In addition to size, also the type of particle is important. A useful classification is to distinguish between metallic, non-metallic, and fibers. Even small metallic particles are often harmful. Since they are hard and electrically conductive, even single particles can lead to the failure of an entire component assembly by means of short circuits or abrasion. Non-metallic particles, e.g. polymers or fibers, are often less problematic. It is useful to treat fibers separately because they are typically very long but thin objects that would otherwise be classified as extremely large non-metallic particles.

A cleanliness inspection system, thus, needs to determine both particle size and type. Standard cleanliness inspection as defined in VDA 19 / ISO 16232 involves washing the sample and filtering the washing medium. The particles, which are

*jan.schuetz@ipm.fraunhofer.de; phone +49 761 8857-742; fax +49 761 8857-224; ipm.fraunhofer.de

collected in the filter, are then optically analyzed with a microscope. Therefore, measurements can only be performed on a sample basis and results are available with huge delay. A 100-percent-analysis, which is often desirable, is not possible.

Optical measurement techniques are in principal suitable to inspect the whole sample surface within the production cycle. In practice, however, they reach their limits. Classical imaging techniques for particle detection, such as dark-field imaging, are limited to flat surfaces because structures, scratches, or rough surfaces will give similar signals as particles. Neither are spectroscopic methods applicable since particulate contaminations often consist of the same material as the samples do. We present new imaging techniques for the detection and classification of particulate contamination on structured surfaces that allow for cleanliness inspection directly on the sample.

METHODS

Stimulated differential imaging

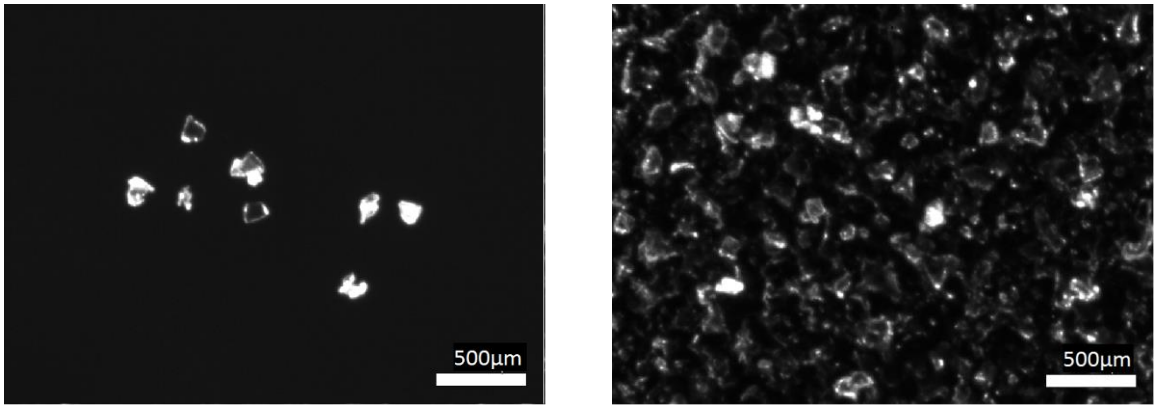

Figure 1. Aluminum particles with 100 – 150 µm size on different surfaces. Particle detection using dark-field imaging works well on the flat glass surface (left) but is limited on the anodized aluminum sheet (right) because surface structures look similar as particles.

A common method for the detection of particles on surfaces is dark-field imaging, where the sample is illuminated under a very flat angle. Smooth surfaces just reflect the illumination light away from the camera. Particles lying on the surface, in contrast, provide a large range of surface angles for the incoming light. Thus, depending on their surface properties, the particles will reflect or scatter parts of the light into the camera. Hence, particles appear bright on a dark surface (Fig. 1, left). Unfortunately, this method is limited to smooth and flat surfaces because structures, scratches, and rough surfaces also deflect light into the camera. Thus, they cannot be distinguished from particles (Fig. 1, right).

This problem can be overcome by exploiting the principal distinguishing feature of particles – they are unbound or weakly bound objects attached to the sample. Thus, applying stimulation mechanisms, such as air blasts or ultrasonic pulses, will result their displacement. Taking one image before the stimulation and another image afterwards, a differential image can be calculated. In this differential image, the displaced particles are visible with high contrast while fix surface structures cancel out. Standard image analysis can then be used to determine particle number and sizes.

This *stimulated differential imaging*[3] is illustrated in Fig. 2. In image a), the particle (green labeled) can hardly be recognized, neither with computer vision nor as a human being. Image b) shows the same area after an air blast was applied. In comparison to image a), it is now clear where the particle initially was located and that it was moved to the side by the air blast. For analysis, a differential image c) is calculated, i.e. $pixel_c(x,y) = pixel_b(x,y) - pixel_a(x,y)$. In this differential image, all fix structures cancel out. Only the areas of the initial and final position of the particle result in non-zero pixel values.

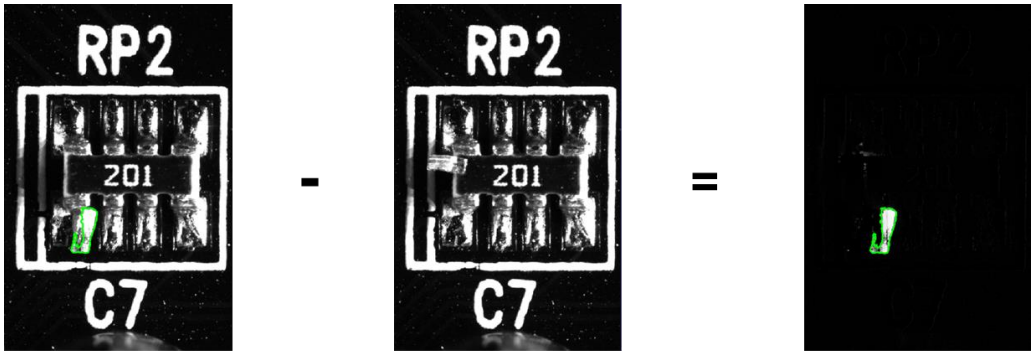

Figure 2. In image a), the particle (green labeled) can hardly be distinguished from surface structure. Image b) was taken after application of an air blast. While the surface structure is equal, the particle moved. Thus, in the differential image c), the surface structure cancels out and only the particle is visible with high contrast.

In general, the differential image can have positive and negative values, which may need to be treated differently depending on the situation. If particles are known to appear bright compared to the background in both original images, e.g. in dark-field illumination, the differential image has positive values at the initial position and negative values at the final position. In this case, the differential image can be restricted to positive values, so that only the initial particle areas remain. This has been done in Fig. 2. If particles can appear both bright and dark, the absolute values of the differential image need to be analyzed. In that case, particles will typically be counted twice because it cannot be distinguished between initial and final position.

Depending on the type of sample and particles, different stimulation methods may be used. In general, mechanical stimuli such as air blasts, sound excitation, and vibration are candidates. In special cases, stimulation with electric or magnetic fields is also conceivable. Strong electric fields should induce a charge displacement in the particles, which in turn causes the particles to move in the field. Magnetic fields only affect magnetic particles. It is useful to integrate the stimulation device either in the measuring head or in the sample holder. In both cases, it must be ensured that the sample itself does not move between the two images, since a shift of one pixel is already visible on the difference image. If slight displacements of the sample cannot be avoided, imaging tools have to be used to realign the images.

Metallic / non-metallic differentiation using gloss

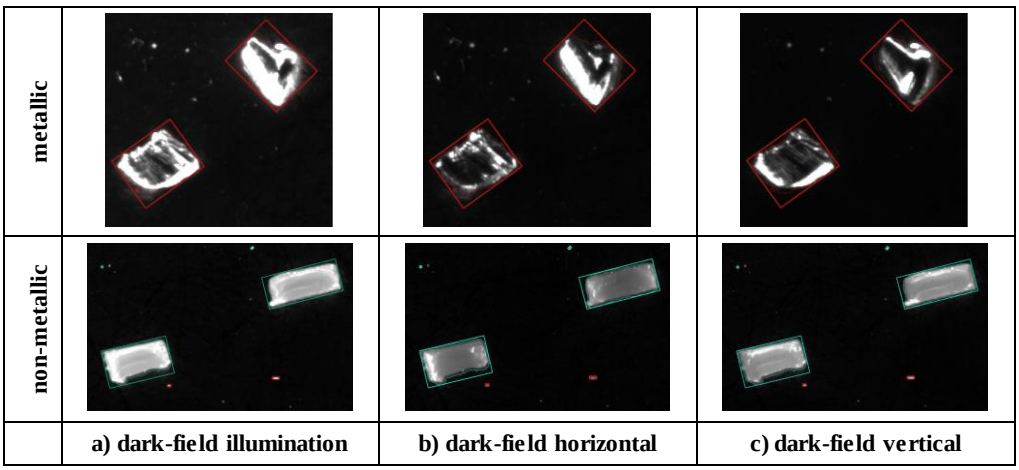

Figure 3. In dark-field images a), the contour of particles, on a flat surface, appears bright on a dark background. When the direction of illumination light is restricted to horizontal b) or vertical c) in image direction, metallic (red labeled) and non-metallic (green labeled) particles behave differently. While non-metallic particles are mainly homogeneously bright, different areas of metallic particles appear bright, due to their glossy surface.

In order to distinguish between metallic and non-metallic particles, the high specularity, which is common to typical metallic contaminations, is exploited by using a newly developed illumination and image-processing scheme. The metallic gloss leads to very bright image regions where light is directly reflected off the metal surface towards the detector. This occurs especially along the particles circumference. By contrast, regions that reflect light away from the detector appear very dark as shown in Fig. 3 a). In contrast to metallic particles, most relevant non-metallic particles exhibit rather diffuse scattering of light instead of forming bright specular reflexes when illuminated by a square of four LED strips in dark-field configuration. This leads to a much more homogeneous brightness distribution of non-metallic particles.

A second effect that shows up when comparing specular reflection and diffuse scattering is the strong difference in directionality of the particle appearance with respect to the position of the light source. Fig. 3 b) displays the identical particles as shown in Fig. 3 a), however, using only the two opposing LED strips that emit light horizontally in image direction. For metallic particles, the appearance is strikingly different when only the vertically aligned pair of LED strips is used, which can be seen by comparison with Fig. 3 c). Instead, the plastic particles shown in the lower row of Fig. 3 appear to produce very similar images in both cases b) and c). They mainly differ in terms of absolute brightness rather than in terms of brightness distribution, where only a slight brightness enhancement of the particle edges facing the light source can be observed.

This strong difference in directionality allows for a robust discrimination between metallic and non-metallic particles[4]. In fact, it turned out to be more suitable than the brightness distribution of a particle illuminated from all four directions.

The development of an algorithm for automatic differentiation between metallic and non-metallic particles requires the similarity of the particle appearance under both illumination directions to be quantified. Different procedures have been tested and best results were obtained using the mathematic procedure of *structural similarity* (SSIM)[5]. This method was originally developed to assess the loss in image quality resulting from image compression. In the presented study, it is used to quantify the similarity of the images recorded with perpendicular directions of illumination.

The *SSIM index* for images x and y is defined as

$$SSIM(x,y) = \frac{(2\mu_x\mu_y + c_1)(2\sigma_{xy} + c_2)}{(\mu_x^2 + \mu_y^2 + c_1)(\sigma_x^2 + \sigma_y^2 + c_2)}$$

with $\mu_{x/y}$ the average of x/y, $\sigma_{x/y}^2$ the variance of x/y, σ_{xy} the covariance of x and y, and $c_{1/2}$ two variables to stabilize the division with weak denominators. The result is a scalar value ranging from -1 to 1, whereby larger values indicate a higher similarity of the images and the value 1 is only reached for identical images.

For convenience, we define a *MetalScore(i)* for particle i with respective image areas x_i and y_i as

$$MetalScore(i) = 100\ \frac{1 - SSIM(x_i, y_i)}{2}$$

The result is a scalar value ranging from 0 to 100, with larger values indicating a larger dissimilarity of the images. The discrimination is achieved by applying a threshold value above/below which particles are considered metallic/non-metallic.

EXPERIMENTAL REALIZATION

A compact particle detector

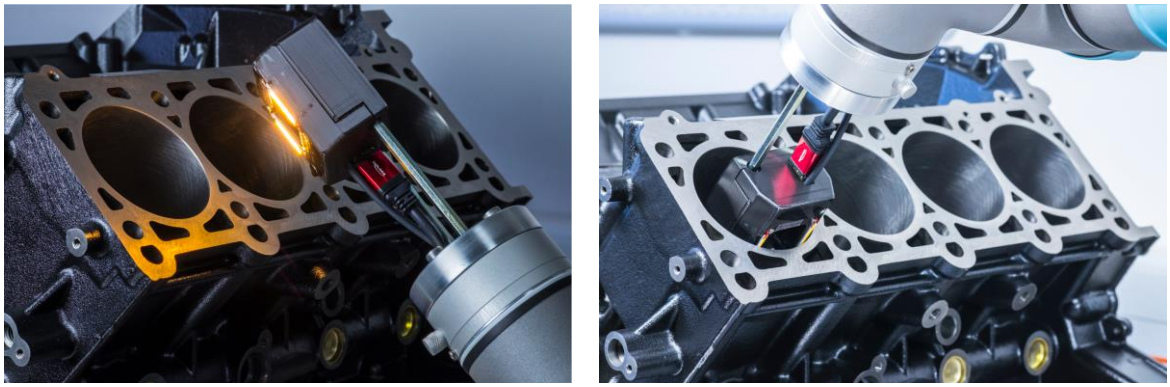

Figure 4. Photos of the sensor head, including camera, illumination, and nozzle for air blasts. The sensor is of size 70 mm × 60 mm × 40 mm and operates with a working distance of 10 mm. It can be attached to a robot to scan the surface of complex samples.

A compact sensor head has been designed, which is shown in Fig. 4. The sensor head contains a 10 MP camera (3800 × 2700 pixel) and a M12 lens that provides a pixel resolution of 5 µm/pixel, corresponding to an image field of 19 × 14 mm². Two squares of LED bars, with each of the four bars individually switchable, are included in the sensor - one square in dark-field and one in bright-field configuration. A switchable nozzle for the application of air blasts is integrated, too. The sensor can be attached to a robot to scan the surface of larger samples. A full measurement cycle, consisting of taking a first image, applying a stimulation method, taking a second image, and image analysis, typically takes less than one second.

Several measurements were performed in order to characterize the optical properties of the sensor. Modulation transfer functions (MTF) were measured using line triplets with different spatial frequencies of a *1951 USAF resolution test chart*[6]. To determine the depth of focus, the chart was moved out of focal plane with a translation stage and the contrast at 20 line pairs/mm was analyzed as a function of displacement.

Stimulation methods

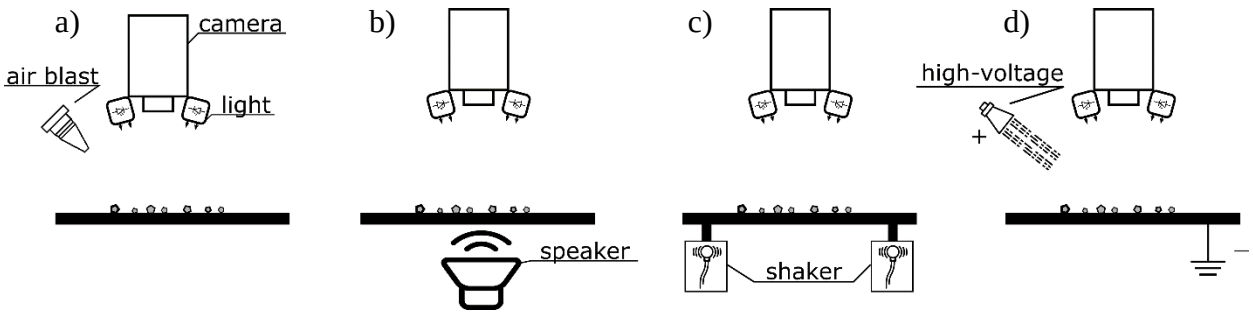

Figure 5. Schematic sketches of all tested stimulation methods: a) air blasts, b) acoustic stimulation with speaker, c) vibrational stimulation with shaker, d) high voltage.

Four different stimulation methods have been tested, as sketched in Fig. 5:

a) For air blast application, blasts with a backing pressure of 1.1 – 1.5 bar were applied for 200 ms using the switchable nozzle of the sensor head.

b) For acoustic stimulation, a speaker was attached below the sample. Sinusoidal tones were then applied for 15 s. The frequency of the applied tones was optimized in the range 0.5 - 2 kHz.

c) For vibrational stimulation, two unbalanced motors were attached to the sample. The motors were driven at about 10000 rpm for 3 s.

d) For electrostatic stimulation, a high voltage generator was used. Ground was connected to the sample and the cathode was in about 2 cm distance from the sample. A high voltage of 30 KV was then applied for several seconds.

The sensor head described in the previous section was used for imaging, with slight modifications if necessary. A rolled aluminum sheet served as sample surface. Particles made from plastic, aluminum, and stainless steel with known sizes were deposited on the sheet. Between 5 and 30 particles were used for each of the size classes 50 – 100 µm, 100 – 150 µm, 150 – 200 µm, 200 – 400 µm, 400 – 600 µm, and 600 – 1000 µm, so that in total between 70 and 100 particles were considered for each method.

The following experiments were performed to characterize the detection rates for each stimulation method. First, a reference image of the clean surface was taken. Then, particles of one size class were deposited and the stimulated differential imaging sequence was performed. This was repeated for all size classes.

The image before stimulation minus the reference image can now be used as an ideal differential image where all particles are visible. For each particle in the ideal image, it is then checked if the particle is also recognized in the differential image resulting from stimulated differential imaging. A particle is considered recognized, if the size class matches.

Particle characterization

A sensor head as shown in Fig. 4, with modified illumination, was used for particle characterization measurements. With identical camera configuration, the lower square of four LED bars was nearly brought into contact with the surface to achieve an ideal dark-field configuration.

The surface of a plane mirror was used as an ideally flat sample surface. Four collections of particles were deposited on the surface to determine classification rates:

1) About 100 large non-metallic particles.
   Purchased standard particles, cut from polypropylene foil, with known size class 200 – 400 µm were used.

2) About 100 small non-metallic particles.
   Particles were filed off from a block of polylactide. The analysis was then restricted in the software to particles with the size determined as 25 – 100 µm.

3) About 100 large metallic particles.
   Purchased standard particles, milled from aluminum, with known size class 200 – 400 µm were used.

4) About 2800 small metallic particles.
   Aluminum particles were used, which were sieved with a sieve with a mesh size of 36 µm.

For each sample, a sequence of five images was taken:

Image1: Illuminated with all four dark-field LED bars.

Image2: Illuminated with two opposing dark-field LED bars.

Image3: Illuminated with the other two opposing dark-field LED bars.

Image4: Illuminated with two opposing bright-field LED bars.

Image5: Illuminated with the other two opposing bright-field LED bars.

Using conventional image analysis tools, *Image1* is used to locate all particles and determine their shapes. For the image areas covered by each respective particle, the metal score using $SSIM(Image2, Image3)$ is calculated. After establishing a suitable threshold value, the particles are classified as metallic/non-metallic for metal score values above/below this threshold value. A second metal score is calculated using $SSIM(Image4, Image5)$ to further improve the algorithm.

RESULTS

Optical characterization of the sensor

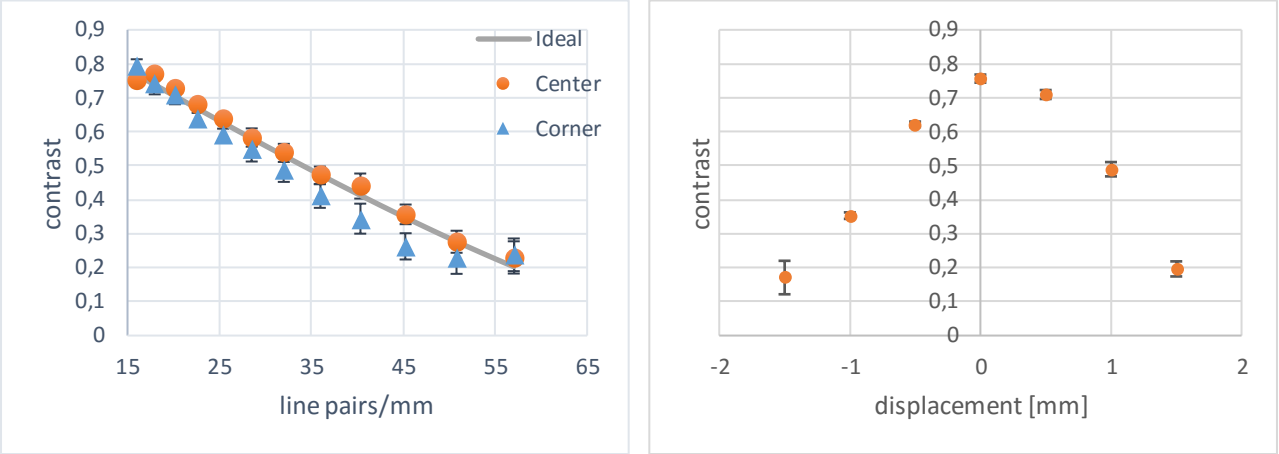

Figure 6. Modulation transfer function (MTF) to characterize the optical resolution (left). Decrease of contrast at 20 line pairs/mm when moving the object out of focal plane to characterize the depths of focus (right).

MTFs measured with the sensor head, one retrieved from the center and one from the corner part of the image, are plotted in Fig. 6, left. The functions nearly match the diffraction limited, ideal curve. A reasonable contrast of 30% is achieved over the whole image for spatial frequencies up to 40 line pairs/mm, i.e. two objects in 1 / 40 mm = 25 µm distance can be well resolved.

The decrease of contrast at 20 line pairs/mm, when moving the object out of focal plane, is plotted in Fig. 6, right. A reasonable contrast of 30% is observed for ± 1 mm, which defines the depths of focus.

Stimulation methods

		particle size [µm]						
		50 - 100	**100 - 150**	**150 - 200**	**200 - 400**	**400 - 600**	**600 - 1000**	**average**
stimulation method	**electrostatic**	-	-	-	-	-	-	**0%**
	vibration	9%	0%	30%	52%	81%	75%	**38%**
	acoustic	66%	60%	66%	37%	100%	98%	**61%**
	air blast	90%	100%	100%	95%	100%	90%	**93%**

Table 1. Recognition rates using stimulated differential imaging with different stimulation methods for various particle sizes.

The observed recognition rates for stimulated differential imaging, using the four different stimulation methods, are compiled in Table 1. Both average values and values for individual particle size classes are given.

For electrostatic stimulation, no particle movement and, thus, no particle detection was observed in the given test case.

For vibrational stimulation, detection rates above 75% are only obtained for particles larger than 400 µm, while smaller particles are not reliably detected. On average, only 38% of the particles were detected.

Acoustic stimulation gives better results. However, the average detection rate of 61% is still too low for a reliable detection system.

The best results are obtained using air blast stimulation. Depending on the specific application, the average recognition rate of 93% is already sufficient or provides a good starting point for further optimization of the process.

Particle characterization

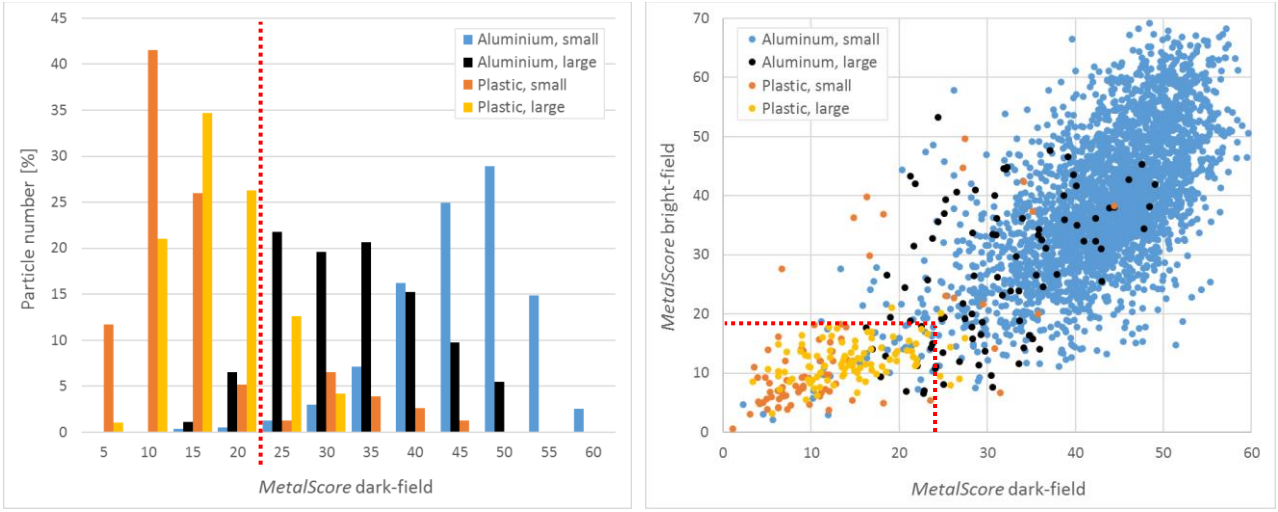

Figure 7. Left: Histogram of metal score values derived from dark-field images for aluminum and plastic particles. Particle numbers were normalized to 100% for each respective group. Right: Scatter plot of metal scores derived from dark-field and bright-field images. Dotted red lines indicate the chosen thresholds.

The resulting distribution of metal score values for aluminum and plastic particles, calculated from the dark-field images $SSIM(Image2, Image3)$, is shown in Fig. 7, left. The values for plastic are clearly below those for metal. However, there is some overlap. Especially some of the small plastic particles reach very high metal scores. One possible explanation is that, when filing the particles, additional metallic particles were detached from the file. In fact, many of the particles in question look like metallic particles in the images. Additional measurements with larger particle numbers and a more careful preparation of small plastic particles will be needed.

The threshold value was set such that more than 90% of the large plastic particles have a smaller value, resulting in a threshold of 23. Particles with metal score above threshold are considered metallic. With this threshold, 84% of the small plastic, 86% of the large aluminum, and 99% of the small aluminum particles are classified correctly. The results are compiled in Table 2.

Type	Size	Number of particles	Correctly classified using dark-field	Correctly classified using dark- and bright-field
Aluminum	36 µm	2795	99%	99%
Aluminum	200 - 400µm	92	86%	92%
Plastic	25 - 100µm	77	84%	78%
Plastic	200 - 400µm	95	91%	92%

Table 2. Percentage of correctly classified particles using dark-field images with *MetalScore* threshold 23 as well as using additional bright-field images with thresholds 19.

The recognition rates can be improved if a second metal score, calculated from the bright-field images $SSIM(Image4, Image5)$, is used in addition. Fig. 7, right, shows a scatter plot of both metal scores. It is apparent that both values are strongly correlated. Values for metal and plastic are well separated in both dimensions. For the falsely classified small plastic particles, both scores are large, which reinforces our belief that these particles are actually metallic.

The threshold for the second metal score was analogously set to 18, so that more than 90% of the large plastic particles have a smaller value. For classification, particles with at least one of the two scores above threshold were considered metallic. This increases the rate of correctly classified large aluminum particles to 92%, while the rate for small plastic particles decreases to 78% (see Table 2).

CONCLUSION AND OUTLOOK

We introduced a new imaging technique, stimulated differential imaging, which allows for detection of particulate contamination on structured surfaces. A compact sensor was developed, that can be attached to a robot to scan the surface of complex samples. The sensor was used to test different stimulation methods. The use of air blasts proved to be the most efficient stimulation method. With the current setup, 93% of all deposited particles were detected correctly.

The presented technology, for the first time, allows real time monitoring of particulate contamination on structured surfaces in the production process. Depending on the specific application, a 100-percent inspection system will require a further improvement of recognition rates. Approaches that are currently being investigated include, for example, the repeated application of air blasts and using blasts with higher pressure.

We further presented a new imaging method to distinguish metallic from non-metallic particles. The method uses gloss as a distinguishing feature and is based on determining the similarity of two images taken under different lighting directions. To implement the method, in addition to image analysis, a sensor system just has to be able to control two different illumination lights. Thus, the method can easily be integrated into existing imaging systems. In particular, a combination with stimulated differential imaging and dark-field imaging is possible.

With the current system, over 90% of the examined particles are classified correctly. The algorithm is currently under optimization and we are confident that further improvement is possible. In comparison to VDA 19 / ISO 16232 standard analysis, the presented classification method has the advantage that it can be performed directly on the sample without the need for washing or other processing of the sample. This allows for a much faster and easier measurement, with a lot more sample throughput.

ACKNOWLEDGEMENTS

Parts of the research leading to these results were supported by the Fraunhofer Internal Programs under Grant No. MEF 835463 and parts of the research were supported by the Federal Ministry for Economic Affairs and Energy on basis of a decision by the German Bundestag.

REFERENCES

[1] VDA Volume 19 Part 1, "Inspection of Technical Cleanliness >Particulate Contamination of Functionally Relevant Automotive Components / 2nd Revised Edition" (2015).

[2] Holz, P., Brandenburg, A., "Ortsaufgelöste Messung filmischer Verunreinigungen", Journal für Oberflächentechnik 58(10), 46-49, (2018).

[3] Schütz, J., Bertz, A., Jetter, V., Beckmann, T., Carl, D., "Vorrichtung zur Partikelanalyse," Patent DE102017104801A1 (2017)

[4] Patent pending.

[5] Wang, Z., Bovik, A. C., Sheikh, H. R., Simoncelli, E. P., "Image quality assessment: from error visibility to structural similarity", IEEE Transactions on Image Processing 13(4), 600-612 (2004).

[6] Edmund Optics, "1951 USAF Glass Slide Resolution Targets", https://www.edmundoptics.com/f/1951-usaf-glass-slide-resolution-targets/12064 (19 June 2019)